

Western University

Scholarship@Western

Chemistry Publications


Chemistry Department

9-2021

Bioaccessibility and reactivity of alloy powders used in powder bed fusion additive manufacturing

Yolanda S. Hedberg

Follow this and additional works at: <https://ir.lib.uwo.ca/chempub>

 Part of the [Chemistry Commons](#)



Full Length Article

Bioaccessibility and reactivity of alloy powders used in powder bed fusion additive manufacturing



Xuying Wang^a, N.V. Srikanth Vallabani^b, Alix Giboin^a, Johan Lundqvist^c, Kim Färnlund^d, Hanna L. Karlsson^b, Yolanda S. Hedberg^{a,e,*}, Inger Odnevall^{a,f,g,*}

^a KTH Royal Institute of Technology, School of Engineering Sciences in Chemistry, Biotechnology and Health, Department of Chemistry, Division of Surface and Corrosion Science, Drottning Kristinas v. 51, Stockholm SE-10044, Sweden

^b Institute of Environmental Medicine, Karolinska Institute, Stockholm SE-171 77, Sweden

^c AB Sandvik Machining and Manufacturing Solutions, Sandviken SE- 811 81, Sweden

^d Amexci AB, Gammelbackavägen 2, Karlskoga SE-691 51, Sweden

^e Department of Chemistry, The University of Western Ontario, 1151 Richmond Str., London, Ontario N6A 5B7, Canada

^f AIMES-Center for the Advancement of Integrated Medical and Engineering Sciences, Karolinska Institutet, KTH Royal Institute of Technology, Stockholm, Sweden

^g Department of Neuroscience, Karolinska Institutet, Stockholm SE-171 77, Sweden

ARTICLE INFO

Keywords:

Corrosion
Metal and alloys
Microstructure
Powder processing
Rapid prototyping

ABSTRACT

Exposure to metal particles via the inhalation route unavoidably takes place at occupational settings during additive manufacturing of metals and alloys. This calls for investigations on possible adverse health effects. This study focuses on virgin and reused powders of three iron- and nickel-based alloy powders (316L, IN718, 18Ni300) widely used in additive manufacturing, and dust powder of 18Ni300 generated during laser melting. Investigations were performed from a physico-chemical and toxicological perspective assessing their bioaccessibility in artificial lysosomal fluid (ALF, simulating lung exposure to respirable particles), corrosion behavior, surface morphology and composition, microstructure, hydrodynamic size distribution in ALF, and *in-vitro* toxicity towards cultured human lung cells. Less than 1% of the powder mass was dissolved from the passive alloys (316L, IN718) under simulated physiological conditions (pH4.5, 37 °C, 24 h), whereas the 18Ni300 iron-nickel alloy showed an active behavior and dissolved completely. Reused powders of 18Ni300 and IN718 showed no, or only minor, differences in surface oxide composition, metal release pattern, and corrosion behavior compared with virgin powders. After reuse, the 316L powder showed an enrichment of manganese within the outermost surface, an increased corrosion current, increased amounts of released iron and an increased fraction of particles with ferritic microstructure, which increased the extent of particle aggregation. All powders showed low, or negligible, cytotoxic potency and reactive oxygen species formation. Powder bed fusion using laser melting can hence affect the chemical, physical, and surface properties of non-fused powders, which, if reused, could influence the properties of the printed part.

1. Introduction

Additive manufacturing (AM), also known as three-dimensional (3D) printing or rapid prototyping, is a ground-breaking technology able to produce complex/customized 3D parts in a wide range of applications from aerospace to medical treatment via computer aided operations [1–5]. Several AM processes, including selective laser melting, binder jetting, and electron beam melting, are available to fabricate metal parts [1,2], of which all use metal powder in the micrometer range as feedstock [6–8]. Powder-based AM technologies offer an advantage in terms of reusability of non-fused powder particles over multiple cycles, which

leads to a more cost-effective and sustainable process [7–10]. In the laser-based AM process, the powder bed is built up layer-by-layer and melted selectively by a laser in a desired pattern to build up a three-dimensional part. Adjacent non-fused powder particles might be partially melted or heated, though this is highly dependent on the geometry of the printed parts. Solidification occurs very rapidly after each melting step [2]. To save costs, companies often reuse non-fused powders within the powder bed. This powder is typically sieved before continuously mixed with virgin powder and re-utilized for printing. It is also common to only work with the same batch of powder and to top-up the machine with fresh powder from the same batch until the batch is

* Corresponding authors at: School of Engineering Sciences in Chemistry, Biotechnology and Health, Department of Chemistry, Division of Surface and Corrosion Science, KTH Royal Institute of Technology, Drottning Kristinas v. 51, Stockholm SE-10044, Sweden.

E-mail addresses: yhedberg@uwo.ca (Y.S. Hedberg), ingero@kth.se (I. Odnevall).

<https://doi.org/10.1016/j.mtla.2021.101196>

Received 23 April 2021; Accepted 14 August 2021

Available online 16 August 2021

2589-1529/© 2021 The Authors. Published by Elsevier B.V. on behalf of Acta Materialia Inc. This is an open access article under the CC BY license (<http://creativecommons.org/licenses/by/4.0/>)

empty, after which the entire batch of used powder is sieved and mixed and reused, thereby having “the same” quality powder when working with a specific batch. Mixing batches is typically only done when several different batches of powder are available, none of which with enough material to complete a print. The new batch is then given a new batch number and analyzed to ensure that the material quality is high enough before usage. If not, it is sent for recycling or used for printing internal demonstrator parts.

Several studies on metal powders used for AM have been conducted, focusing on how the powder properties change upon reuse and how the use of recycled powder influences the final properties of the printed parts. This has for instance been investigated for titanium (Ti) and aluminium (Al) alloys, nickel-based alloys (e.g. Inconel 718), cobalt-chromium (Co-Cr alloys) and stainless steel [2,7–12]. These studies address how repeated use of non-fused particles influence parameters such as microstructure, particle size distribution, degree of oxidation, and flowability. Reused non-fused particles have been shown to undergo dynamic thermal interactions with the energy source during manufacturing, resulting in variable particle behavior and in some cases causing reduced quality of printed parts [7,10,13,14]. Studies of reused powder particles (up to 30 cycles) have shown minor changes in terms of particle size distribution and bulk composition, but a slight increase in oxygen content compared with virgin powders [7,9,10,15,16]. These changes have been reported to be minor, and the reuse of non-fused powders possible for several cycles. Changes in surface oxide composition or differences in bioaccessibility (metal release) of the powders in contact with physiologically relevant fluids upon human exposure have though not earlier been explored.

Although current AM machines are usually encapsulated and equipped with exhaust-air filtration, AM workers might be at risk for exposure to metallic particles during handling, use, and disposal of the powders [17–19]. The potential human exposure to airborne metal-containing particulates (including nanoparticles and their aggregates) forming during AM have been associated with an increased risk for respirable tract diseases including asthma and lung inflammation [17–21]. For example, both nickel (Ni) and cobalt (Co) are common metals in AM feedstocks and classified by the European Chemical Agency (ECHA) as respiratory sensitizing materials [22,23]. Currently, there is no consensus regarding potential hazards of micrometer- and nanometer-sized particles, or non-intentional particles generated during AM processes. However, in view of the latest report of the International Agency for Research on Cancer (IARC) on welding fumes [24,25], concluding on an increased risk of lung cancer independent of welding method, the AM safety should be taken seriously. While there are no regulatory limit values set for hazardous exposure to inhalable particles during AM, the Finnish Institute of Occupational Health (FIOH) has defined a target level of 2 mg/m³ (inhalable fraction) for workplace dust concentrations [26]. This calls for the necessity to quantify and characterize metal powders used, and non-intentionally generated, during various AM processes from a physical, chemical, and toxicological perspective [17,27], assessing their bioaccessible fractions. Bioaccessibility is in this context defined as the extent of released metals into physiologically relevant fluids, becoming potentially available for human uptake [28,29].

Triggered by substantial knowledge gaps, the objectives of this study were to assess differences between virgin and reused metal alloy powders of 316L, IN718 and 18Ni300 used in AM powder bed fusion processes (selective laser melting) from a physicochemical, microstructural, surface composition, bioaccessibility, and *in-vitro* toxicity perspective.

2. Materials and methods

2.1. Materials

Virgin (as-received feed stock) and reused non-fused gas-atomized metal alloy powders of an austenitic stainless steel AISI 316L (316L), a nickel-based Inconel alloy (IN718), and a high strength steel (18Ni300)

were investigated. These alloy powders are commonly used in different powder bed fusion AM applications, in this study using selective laser melting. Their nominal composition is given in Table 1 based on supplier information. The powders were collected and supplied by Siemens, Amexci, and Sandvik, respectively, all in Sweden.

The reused powders of this study had been sieved and reused at least once. For the alloy 18Ni300, dust was collected directly from the manufacturing chamber air (a dust layer formed on the chamber walls with the flow of argon passing).

2.2. Bioaccessibility studies

Ultrapure water (resistivity of 18.2 MΩcm) was used in all cases as solvent, and all experimental equipment and vessels were acid-cleaned (10% HNO₃ for at least 24 h) followed by rinsing (four times) in ultrapure water before dried in ambient laboratory air. The powders were exposed to artificial lysosomal fluid (ALF, pH4.5) at 37 °C for 24 h at a particle mass to solution volume ratio (loading) of 0.1 g/L. This loading is recommended by the OECD transformation/dissolution protocol for aquatic acute tests [30] and has in previous studies been shown to be low enough to minimize the effect of particle agglomeration [31,32]. The ALF solution was chosen to mimic a relevant inhalation exposure scenario, as it represents the intracellular inflammatory conditions in lung cells following phagocytosis by macrophages [32,33]. ALF is composed of 20.8 g/L citric acid, 6.00 g/L NaOH, 3.21 g/L NaCl, 0.128 g/L CaCl₂·H₂O, 0.090 g/L disodium tartrate dihydrate, 0.086 g/L sodium pyruvate, 0.085 g/L sodium citrate, 0.077 g/L trisodium citrate dihydrate, 0.071 g/L Na₂HPO₄, 0.059 g/L glycine, 0.0497 g/L MgCl₂, 0.039 g/L Na₂SO₄, adjusted to pH 4.5 by NaOH. Triplicate samples of each powder with one corresponding blank sample (without powder) were exposed in acid-cleaned polymethylpentene (PMP) Nalgene jars in dark conditions in an incubator (Edmund Bühler GmbH TH30, Bodelshausen, Germany) set at 37 ± 1 °C with gentle bilinear agitation (inclination 12 °, 22 cycles/min). After exposure, the upper part of the test solution was transferred to a new test tube and centrifuged (3000 g for 10 min) to separate the particles from the solution. The supernatant was then acidified by 65% HNO₃ to a pH less than 2 for metal release analysis. Further experimental details are given elsewhere [28].

Total amounts of released metals in solution were analyzed by means of inductively coupled plasma sector field mass spectrometry (ICP-SFMS, ELEMENT 2, Thermo Scientific). The limits of determination of the metals of interest in the ALF solution were 0.05 µg/L for Co and Nb, 0.2 µg/L for Mo, 0.5 µg/L for Cr, Mn, and Ni, 1 µg/L for Ti, 5 µg/L for Al and 10 µg/L for Fe. Mean value of three independent samples are presented for each powder with the respective blank sample subtracted. Released amounts of metals expressed as µg/µg are based on blank-corrected concentrations of released metals (µg/L) normalized to the solution volume (*L*) and the powder sample weight (µg).

2.3. Particle and surface characterization

Size, surface morphology, shape and elemental composition of the different powders were characterized by means of scanning electron microscopy combined with energy dispersive spectroscopy (SEM/EDS using a FEI XL30 instrument and INCA software, 20 kV). The powders were fixed on carbon tape. The microstructure of the virgin and reused non-fused 316L powders was characterized using electron backscatter diffraction (EBSD, using a digital HKL Nordlys II F + camera attached to a FEG-SEM Leo1530 instrument upgraded to Zeiss Supra 55) using an aperture of 120 µm, a working distance of 10 mm, and a voltage of 15 kV.

Determination of specific surface area (m²/g) and hydrodynamic particle size distribution in ALF was made using laser diffraction (DLS, Malvern Mastersizer 3000). Refractive indexes of alloys (2.757) and water (1.33, as the solvent), as well as the alloy densities (316L: 8.0 g/cm³,

Table 1
Nominal bulk composition (wt. %) of the investigated alloy powders based on supplier information.

Grade	C	Cr	Ni	Co	Ti	Al	Mo	Mn	Nb	Si	Fe
316L	< 0.03	17–19	13–15	N/A	N/A	N/A	2.25–3	< 2	N/A	< 0.75	Bal.
IN718	0.05	18.75	52.16	0.14	0.95	0.52	3.02	0.02	5.13	0.02	Bal.
18Ni300	0.011	0.23	17.7	9	0.75	0.1	4.9	0.07	N/A	0.07	Bal.

N/A - no data available; Bal. – balance.

18Ni300: 8.05 g/cm³, IN718: 8.19 g/cm³) were used as input parameters for the calculation as described in [28]. At least triplicate measurements were performed for each powder.

Surface compositional analysis of the powders was performed by means of X-ray photoelectron spectroscopy (XPS, UltraDLD spectrometer, Kratos Analytical) using a monochromatic Al K α X-ray source (150 W) on areas sized 0.7 \times 0.7 μ m. Curve fitting was performed using a linear background correction and peak deconvolution using the Gaussian-Lorentzian function. Wide spectra were run to determine elements present in the outmost surface oxide (approx. 5 nm), and high-resolution spectra (20 eV pass energy) were acquired for Cr 2p, Ni 2p, Fe 2p, Mn 2p, Ti 2p, Nb 2p, corrected to the C 1s contamination peak at 285.0 eV. Measurements were performed at duplicate powders of each material mounted on adhesive carbon tape. Results are presented as the relative mass content of oxidized metals within the outermost surface oxide for independent duplicate samples of each powder.

2.4. Electrochemical measurements

Potentiodynamic polarization measurements were performed in ALF to investigate differences in corrosion resistance at ambient room temperature using a PARSTAT MC Multichannel potentiostat (Solartron analytical). Approximately 5 mg of each powder was immobilized on a paraffin-impregnated graphite electrode (PIGE) covering a surface area of 0.20 cm² [34]. An Ag/AgCl saturated KCl electrode was used as reference electrode and a platinum wire as the counter electrode. After 1 h at open circuit potential (OCP), the potential was polarized from -0.2 to 1.0 V vs. OCP at a scan rate of 1 mV/s. At least two replicate measurements were performed for each powder.

2.5. Toxicological evaluation

Human bronchial epithelial cells (HBEC3-kt, originally from ATCC) were cultured in T75 flasks pre-coated with collagen (32 μ g/mL, Type I, PureCol®, Advanced BioMatrix Carlsbad, CA) in serum-free medium containing 50% LHC-9 (Laboratory of Human Carcinogenesis-9, Gibco, Carlsbad, CA) and 50% RPMI (Roswell Park Memorial Institute, Sigma Aldrich, St. Louis, MO). The medium was supplemented with 1% PEST (penicillin-streptomycin, Gibco, Buffalo, NY) and 1% L-glutamine (2 mM, Gibco, Buffalo, NY). Cells were maintained at 37 °C in a standard humidified incubator supplied with 5% CO₂.

The investigated powder particles were weighed in glass vials, and resuspended in ultrapure water at a loading of 1 mg/mL followed by bath sonication for 20 min. After sonication, this stock solution was immediately diluted to the individual doses in cell culture medium.

Cytotoxicity assessment of the powders was determined by using the Alamar blue assay. Briefly, 1.0 \times 10⁴ cells/well were seeded in a 96 well plate (pre-coated with collagen) and kept for 24 h at 37 °C in a CO₂-supplied humidified incubator. Cells were exposed for 24 and 48 h to the alloy powders in five concentrations (doses): 10, 25, 50, 75 and 100 μ g/mL. After exposure, the cell medium was removed and 10% Alamar blue reagent prepared in fresh medium (Alamar Blue, Invitrogen, Carlsbad, CA) was added to the cells. After 2 h incubation at 37 °C, the fluorescence was read using a microplate reader (Tecan, San Jose CA, Infinite F 200, Software: Magellan 7.2) at 540/590 nm excitation/emission. Three independent measurements were performed for each powder and dose.

Acellular ROS generation was assessed using the DCFH-DA assay (2',7'-dichlorodihydrofluorescein diacetate, Sigma Aldrich, St. Louis, MO) [35]. ROS generation from the particles was determined in presence and absence of HRP (horse radish peroxidase, Sigma Aldrich, St. Louis, MO), sensitive to H₂O₂. The cleavage of the diacetate group was made by incubating 40 μ L DCFH-DA (5 mM in dimethyl sulfoxide) in 1.6 mL 0.01 M NaOH for 30 min at dark conditions, followed by the addition of 8 mL PBS (phosphate buffered saline, KH₂PO₄ (1.05 mM), NaCl (155.17 mM) and Na₂HPO₄·7H₂O (2.96 mM), pH7.4, Thermo Fisher Scientific) to neutralize the reaction. 25 μ L of particle suspensions were mixed with 75 μ L DCFH solution (final particle concentrations of 10 and 50 μ g/mL) in a black 96 well plate and incubated at 37 °C for 30 min. In case of reaction with peroxidase, HRP (final concentration 2.2 U/mL) was added to the DCFH solution and finally incubated with the powder particles. After incubation, the fluorescence was recorded at 485/535 nm excitation/emission using a Tecan plate reader. The increase in ROS was calculated and compared to the control (PBS added to DCFH or DCFH-HRP solutions). Three independent measurements were performed for each powder.

2.6. Statistical evaluation

An un-paired Student's *t*-test with unequal variance (KaleidaGraph v. 4.0) was applied for statistical analysis of the bioaccessibility and particle characterization results. For the toxicity, two-way analysis of variance followed by Dunnett's multiple comparisons test was used to test for statistically significant differences between exposed and control samples. A *p*-value less than 0.05 was considered as statistically significant difference.

3. Results and discussion

3.1. Metal release in ALF (bioaccessibility)

The extent of dissolution/release of metals (Fe, Cr, Ni, Mo, Mn, Co, Ti, Al, Nb, depending on alloy) from the different powders (the bioaccessible pool of metals) into ALF (24 h, 37 °C) was assessed and expressed as their released amounts per exposed powder mass. For the 316L and IN718 powders, less than 1 wt. % of the powder mass was released into ALF (<0.01 μ g/ μ g), while 18Ni300, the high strength alloy, was almost completely dissolved within the same time period (\approx 1 μ g/ μ g) (Fig. 1). Minor differences in metal release were observed between virgin, reused (non-fused), and dust powders (*p* > 0.05) of 18Ni300. Less than 0.1% of the powder mass was dissolved in the case of the IN718 alloy with slightly more metals released from the reused powder. However, in the case of the 316L powder, a 50-fold increase in Fe release was noted for the reused (0.00962 \pm 0.016 μ g/ μ g) powder compared with the virgin powder (0.00019 \pm 0.00008 μ g/ μ g). However, this difference was not statistically significant (*p* > 0.05), which is further discussed below.

3.2. Particle characterization

3.2.1. Particle morphology and size distribution in solution

Differences in particle morphology (by means of SEM), size distribution and specific surface area (by means of DLS) in ALF of the virgin, reused and dust powders are illustrated in Fig. 2. All particles showed a spherical morphology and a particle size distribution in solution which

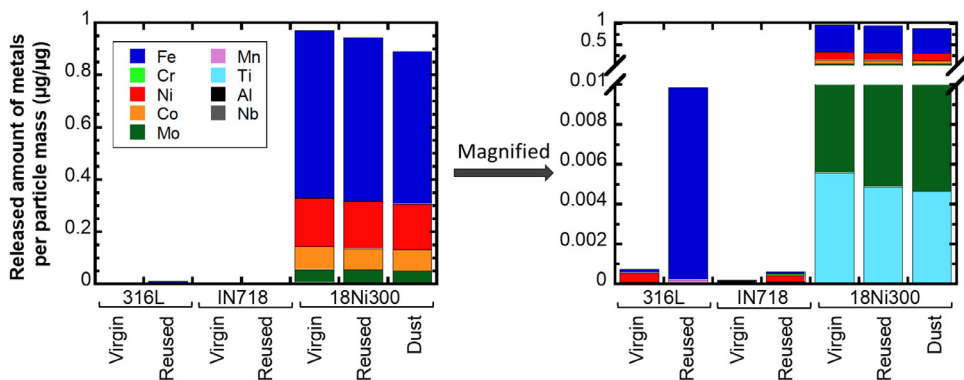


Fig. 1. Metal (Fe, Cr, Ni, Co, Mo, Mn, Ti, Al, and Nb) release [per particle mass ($\mu\text{g}/\mu\text{g}$)] of virgin, reused, and dust alloy powders (316L, IN718, 18Ni300) exposed to ALF (pH4.5, 37 °C) for 24 h. Mean value of three independent samples for each powder. Magnified data to the right. Raw data are presented in Table S1 in the supplementary material.

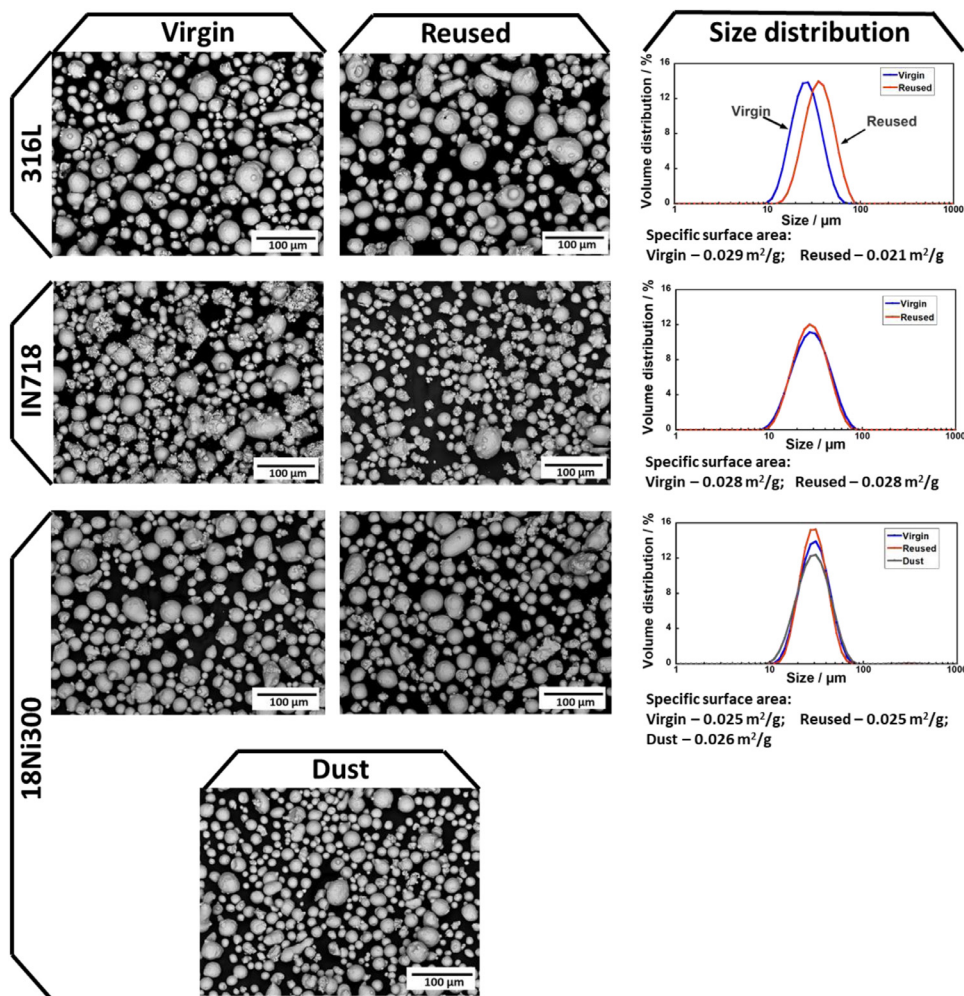


Fig. 2. Particle size and morphology of virgin, reused, and dust powders of 316L, IN718, and 18Ni300 determined by means of SEM (left), and hydrodynamic particle size distributions (by volume) and calculated specific surface areas (m^2/g) of the same powders exposed in ALF (pH4.5) determined by means of laser diffraction (right). The results reflect mean values of at least three measurements of unique samples with a standard deviation of less than 10%.

can be considered inhalable (less than 100 μm in diameter [36]). The SEM images revealed for most powders the presence of smaller sized particles ($<10 \mu\text{m}$) and small-sized satellites present on larger-sized particles. Both the SEM images and the results of the hydrodynamic size distribution measurements in ALF conveyed a relatively broad particle size distribution (between 1 and 100 μm), with a maximum at typically 30 μm for most powders, except for the reused 316L powder with a maximum at 38 μm (Fig. 2). Calculated specific surface areas based on the DLS measurements varied from 0.021 to 0.029 m^2/g , with the most significant difference observed between the virgin and reused 316L powders, for which the recycling process resulted in an evident shift in hydrodynamic size distribution towards larger sizes in ALF (Fig. 2).

Similar trends with increased particle size (either by means of SEM or laser diffraction analysis) of reused powder particles have previously been reported for 316L and Ti6Al4V [7,13]. No significant differences in hydrodynamic size for reused compared with virgin powders were observed for the IN718 and 18Ni300 powders (Fig. 2). Nevertheless, microstructural and surface morphological differences were observed by means of SEM at higher magnification (Fig. 3) for both the 316L and IN718 powder. These reused powders revealed a smoother surface (lack of dendrites) and obvious sintering of small satellite particles to the larger-sized particles. These observations agree with literature findings [7,15,16] and are believed to be a result of melting and solidification events caused by the laser thermal treatment.

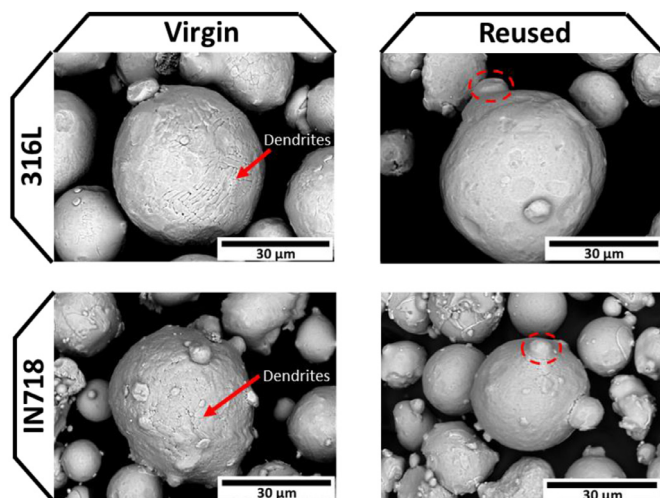


Fig. 3. SEM images of virgin and reused powder particles of 316L (top) and IN718 (bottom) visualizing differences in microstructure and surface morphology.

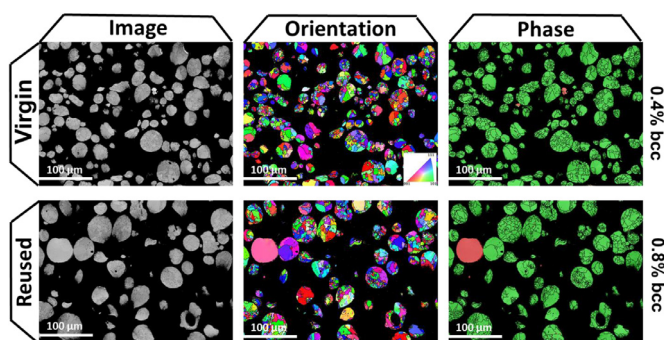


Fig. 4. Differences in crystallographic structure of virgin (top) and reused (bottom) 316L powder particles (left) by means of EBSD, showing the orientation (inverse pole figure mapping in the x-direction) of different grains (middle) and phases (right, green – austenite, fcc; red – ferrite, bcc) in different particles.

Since the ferritic fraction (body-centered cubic, bcc, ferromagnetic properties) within the austenitic microstructure (face-centered cubic, fcc) of the 316L powder can increase upon very rapid solidification [7,37], EBSD measurements were conducted to assess if the virgin and reused 316L powders showed any differences in microstructure (Fig. 4). As expected, both powders revealed a predominantly austenitic structure (fcc, green), though the reused powder showed a slightly larger grain size and a 2-fold increased ferritic fraction (from 0.4 to 0.8%) (bcc, red). The ferritic particles of the reused powder were single-crystalline, as evident from the orientation mapping images (Fig. 4, middle). Compositional analyses by means of EDS supported the conclusion on ferritic particles formed through rapid solidification, showing a different composition for the ferritic particles of the virgin powder compared to the reused powder. The single-crystalline ferritic particles in the reused powder had the same composition as the other austenitic particles (same composition as 316L powder as a whole), whereas the ferritic particles of the virgin powder in contrast were rich in manganese and oxygen, accompanied by some chromium, and hence indicative to be caused by impurities.

These observations suggest the formation of ferritic (retained ferrite) single-crystalline 316L particles within the reused non-fused powders due to the very rapid solidification procedure during the powder bed fusion AM process [7,14,37,38]. Their presence was further confirmed by using a magnet. The magnetic fraction was clearly greater for the reused 316L powder compared to the virgin powder, explaining their

greater hydrodynamic size in solution due to magnetic attraction. The IN718 powders were in contrast non-magnetic, whereas the 18Ni300 powders were entirely magnetic. This is expected from their respective austenitic and martensitic microstructures (martensitic for rapidly cooled gas-atomized powder [12]).

3.2.2. Particle surface oxide composition

The relative oxidized metal composition of the outermost surface oxides of the investigated powders is presented in Fig 5. The results clearly show for all powders a different surface oxide composition compared with the bulk composition (in Table 1) and a slightly different composition between the surfaces of virgin and reused powder particles.

The surface oxides of virgin and reused 316L powder were predominantly composed of Fe(III)-oxides (710.8 ± 0.1 eV, 712.7 ± 0.3 eV), Cr(III)-oxides (576.4 ± 0.1 eV, 577.5 ± 0.5 eV), and Mn(III/IV)-oxides (641.8 ± 0.1 eV, 643.7 ± 0.2 eV) [39], Fig. 5a. Surface enrichment of Mn was evident for both powders and attributed to the large affinity of Mn to oxygen and its tendency to diffuse to the surface during the gas-atomization and AM processes. The enrichment of Mn was slightly higher for the reused powder compared with the virgin powder [34,40]. The reused powder of 316L also showed a somewhat reduced fraction of oxidized Cr, possibly due to its preferential evaporation at high temperature [41]. The slightly increased fraction of oxidized Fe oxide was not statistically significant (Fig. 5a). Increased concentrations of oxidized Fe have been reported for the surface oxide of reused 316L powder [7], and may explain the observation of somewhat increased levels of dissolved Fe from the reused powder upon exposure in ALF, Fig. 1.

The IN718 powders clearly showed the surface enrichment of Ti (458.3 ± 0.05 eV) and Nb (203.6 ± 0.04 eV, 206.8 ± 0.02 eV) as compared to the bulk composition (Table 1). These binding energies indicate the presence of Ti(IV)-oxides (TiO_2) and Nb(II/IV)-oxides (Nb_2O_5) [42,43]. The presence of Nb in the outermost surface of IN718 has been reported in other studies [41,44] and is explained by effects induced by high cooling rates.

In accordance with literature findings for 18Ni300 [12], all 18Ni300 powders investigated in this study revealed oxidized Fe (710.5 ± 0.1 eV, 712.6 ± 0.1 eV) and Ti (455.9 ± 0.2 eV, 458.2 ± 0.03 eV) in the outer surface, Fig. 5c. Observed binding energies indicate the presence of Fe(III)- and Ti(II/IV)-rich oxides in different proportions [39,42]. The reused and dust powders showed slightly higher surface fraction of Fe-oxides compared to the virgin powder. The presence of Ti-oxides in the outermost surface, as a result of its high affinity to oxygen [9] was nevertheless not sufficient to hinder almost complete dissolution of the powders in ALF, Fig. 1. Small differences in surface oxide composition were observed between the virgin and reused powders for all alloys investigated. The barrier properties of the surface oxides within the outermost surface were sufficient to minimize the release of metals into ALF (< 1% of the total mass), Fig. 1, from 316L and IN718 powders.

3.3. Corrosion behavior

Results of the potentiodynamic polarization measurements of the 316L, IN718 and 18Ni300 powders (at least duplicate samples of each alloy) performed after 1 h stabilization at the open circuit potential (OCP) in ALF are shown in Fig. 6. Corresponding corrosion parameters (corrosion potential - E_{corr} , corrosion current - I_{corr} , and anodic branch current - I_{ab}) of each alloy are summarized in Table 2. The corrosion potential was defined as the potential where the current was closest to zero, while the corrosion current, not normalized to the surface area, was estimated by Tafel approximation. The powder-covered surface area was in all cases 0.2 cm^2 , but since the effective surface area of the powder is unknown, the current is presented instead of the current density. Since a passive current can only be estimated for passive materials, we defined the current at a potential of +200 mV to the corrosion potential and denoted it as the anodic branch current to enable comparisons between the alloys.

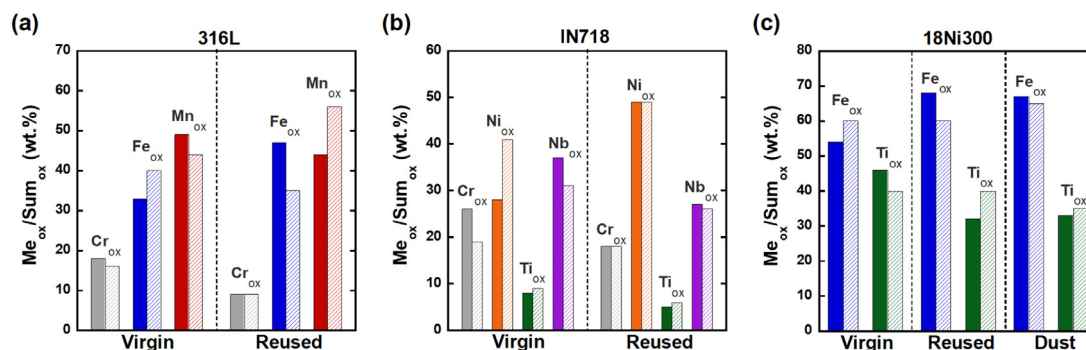


Fig. 5. Relative oxidized metal content (wt.%) in the outermost surface oxides of the investigated powders determined by means of XPS. The two bars represent independent duplicate samples of each powder (particles covering a surface area of $\approx 0.4 \text{ mm}^2$).

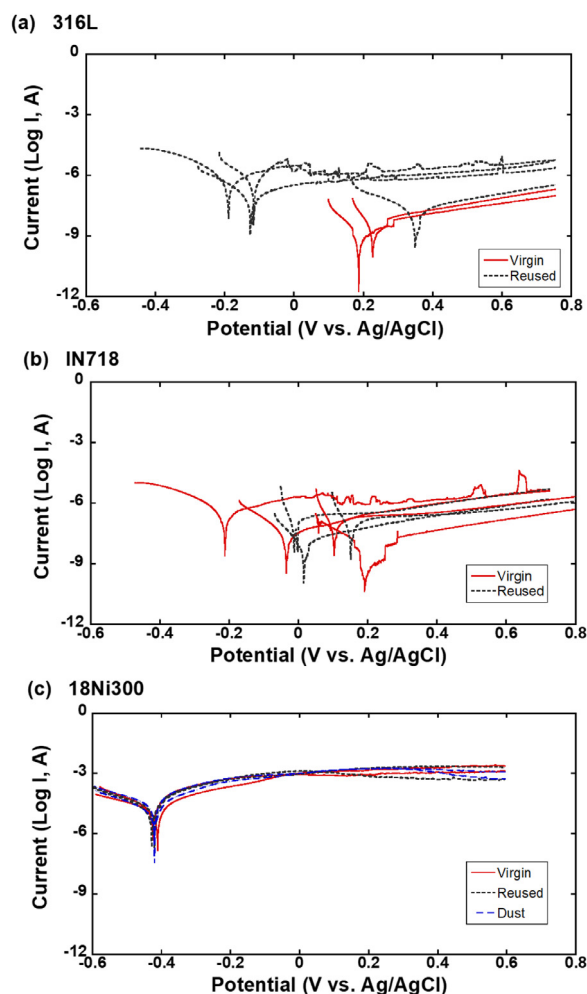


Fig. 6. Polarization curves (1 mV/s scan rate) of 316L (a), IN718 (b) and 18Ni300 (c) powders exposed in ALF (pH4.5, room temperature) after 1 h stabilization at OCP. Note that the current is not normalized to the surface area, but determined for all powders for the same powder-covered surface area (0.2 cm^2) on the PIGE electrode. At least two replicate measurements (same color and line styles in the graphs) were performed for each powder.

For 316L (Fig. 6a), the reused powders were more electrochemically active than the virgin powder in ALF. The former powder showed slightly lower E_{corr} , higher I_{corr} and higher I_{ab} ($p > 0.05$) than the latter, even though large deviation in E_{corr} was evident due to one outlier measurement (Table 2, Fig. 6a). These results indicate that the reused

Table 2

Corrosion potential - E_{corr} , corrosion current - I_{corr} , and anodic branch current - I_{ab} (defined as the current at a potential +200 mV from the corrosion potential) of each investigated alloy powder evaluated from their polarization curves (Fig. 6). Mean values and standard deviations presented for two to four independent measurements of each powder.

Powder		E_{corr} (mV)	I_{corr} (μA)	I_{ab} (μA)
316L	Virgin	215 ± 25	0.0015 ± 0.00050	0.019 ± 0.0081
	Reused	-18 ± 247	0.24 ± 0.23	1.16 ± 1.12
IN718	Virgin	11 ± 179	0.097 ± 0.12	0.62 ± 0.88
	Reused	53 ± 89	0.075 ± 0.053	0.21 ± 0.13
18Ni300	Virgin	-419 ± 13	11 ± 0.66	334 ± 179
	Reused	-424 ± 4	15 ± 7	457 ± 24
	Dust	-423 ± 2	14 ± 4	426 ± 118

powder particles were more susceptible to corrosion compared with the virgin powder. This could be attributed to observed differences in crystallographic structure (Fig. 4) and are in line with the metal release findings (Fig. 1). No statistically significant differences in polarization characteristics ($p > 0.05$) were observed between virgin and reused IN718 powders, which both showed a large variability between the measurements (Table 2 and Fig. 6b). The observation of current fluctuations for the passive powders (316L and IN718) are typical for electrochemical measurements of particles and attributed to effects induced by some particles being more active than others [34]. This results in an increase in current prior to their complete dissolution or detachment followed by a reduced current. All 18Ni300 powders, independent of type, showed an evident active corrosion behavior (Fig. 6c), with significantly lower E_{corr} , higher I_{corr} and I_{ab} ($p < 0.05$), a substantially lower corrosion resistance compared with the other alloy powders (Table 2). Similar to the metal release findings, Fig. 1, there were signs of complete dissolution of the anodically polarized 18Ni300 powders (Fig. 6c), as the current in some cases decreased due to a limited amount of remaining powder.

3.4. Toxicological evaluation

The viability of human bronchial epithelial cells (HBEC) exposed to the powders for 24 and 48 h was explored for 5 different particle doses varying from 10 to 100 $\mu\text{g}/\text{mL}$ (Fig. 7).

The mitochondrial activity assessed from the Alamar blue assay revealed no statistically significant cytotoxicity (no decrease in viability) for any of the powders compared to control. Acellular ROS generation of the powders using DCFH-DA in absence and presence of HRP is presented for two particle doses (10 and 50 $\mu\text{g}/\text{mL}$) in Fig. 8a and b, respectively.

No distinct increase in ROS generation was observed for any of the powders compared to the control. These findings are in line with our previous investigations showing no effect on cell viability (A549 cells) following exposure to micrometer-sized 316L or IN718 particles [45,46].

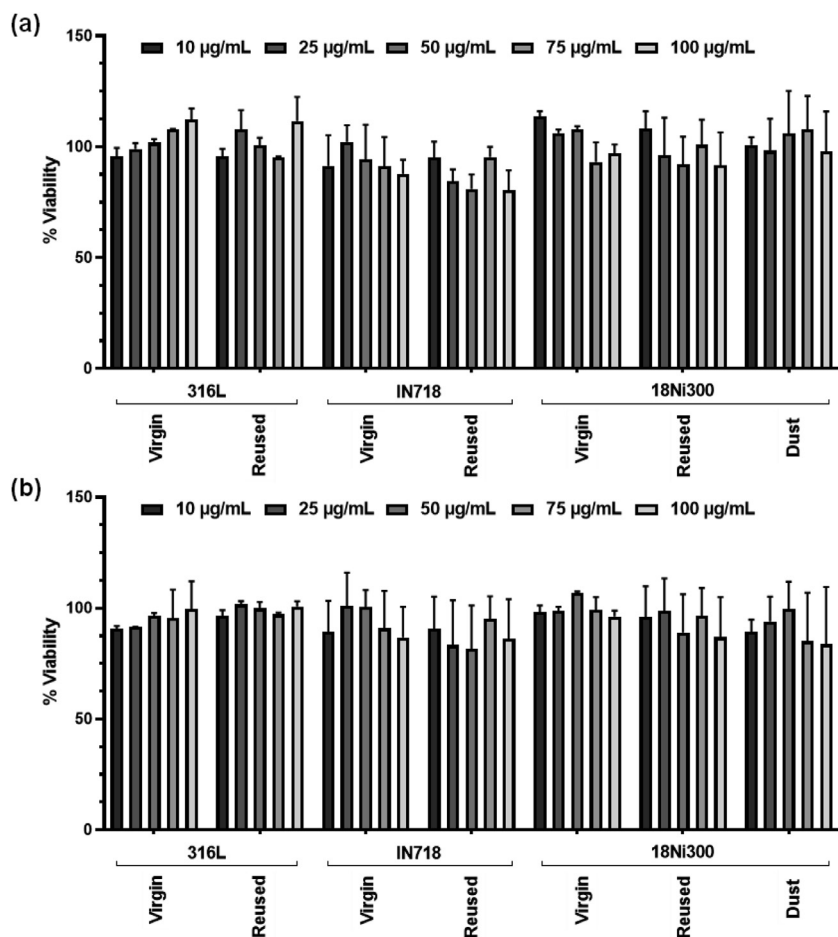


Fig. 7. Cell viability of HBEC exposed to 316L, IN718, and 18Ni300 powders for 24 (a) and 48 h (b). The results show mean values and standard deviations based on three independent measurements of each powder and dose. The viability of control cells was counted as 100% (not shown in graph).

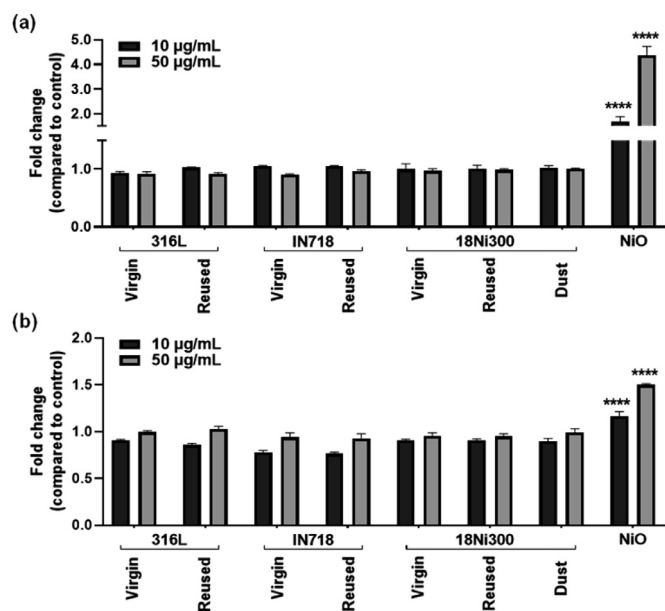


Fig. 8. ROS generation by 316L, IN718, and 18Ni300 powders in absence (a) and presence (b) of HRP. The reaction was carried out in cell-free conditions at 37 °C for 30 min in PBS. Results are represented as mean values and standard deviations of triplicate measurements of each powder compared to control (considered as 1.0, not shown in graph). Results of the positive control (NiO nanoparticles) is included for comparison. Asterisks indicate a significant ($p < 0.001$) difference compared to control.

Furthermore, our previous studies showed no signs of ROS generation of similar IN718 powder as in this study [46], though a small increase of DNA strand breaks was noted for a 316L powder sized $<4 \mu\text{m}$ [45]. Since no particle uptake investigations were performed in this study, it is thus possible that the relatively large particle sizes of the three alloy powders might have hindered cell uptake and therefore limited any toxic effects. More studies are needed to fully explore any toxicological potential of these particles with a focus on effects including genotoxicity and inflammation. A 28 day inhalation study with rats exposed to the same $<4 \mu\text{m}$ sized 316L particles [45] showed, however, no signs of inflammation despite accumulation of metal particles in the lung lobes [47]. Studies are on-going investigating the interplay between particle characteristics and toxicity of smaller-sized particles emitted during the AM process. The importance of such measurements has further been triggered by recent findings, which show emissions of particles in the size range from 10 nm to 10 μm or larger size during post-processing and specific work tasks at AM occupational settings [48]. Taken together, generated results indicate relatively low toxicity towards HBEC and a low ability to generate ROS of the powders tested. No differences between the virgin, reused and dust powders were observed by these toxicological methods.

3.5. Further discussion

Two of the investigated alloys, the stainless steel 316L and the nickel-based Inconel alloy IN718 were shown to be passive (high corrosion resistance) at simulated inhalation conditions, while the high strength iron-nickel alloy 18Ni300 showed a very low corrosion resistance and dissolved completely after 24 h in ALF. All alloy powders were in the inhalable size range with comparable particle size distribution centered

around 30 μm . Their size distribution is probably the main reason why no cytotoxic effects and no ability to generate ROS were observed *in-vitro*. A smaller size ($<4 \mu\text{m}$) would be required for efficient cell uptake [49–51], which is often required to observe cytotoxic effects induced by metal particles. Other reasons for the lack of observed *in-vitro* effects could be inhomogeneous particle distribution during the tests, due to the large size and possible agglomeration of the particles [52], slow transformation/dissolution of particles if taken up by the cells, which could result in chronic effects (not investigated in this study), and/or possibly a change of chemical speciation of the released metals, hindering uptake as judged from data in similar cell media [53,54].

While the 18Ni300 alloy powder was neither found to be cytotoxic nor to produce ROS in this study, its high corrosion rate and bioaccessibility deserves further attention. The 18Ni300 powders completely dissolved after 24 h in ALF compared to less than 1% of the powder mass for the two passive alloys. Complete dissolution of the 18Ni300 powders follows the release of predominantly Fe, Ni, Co, Mo and Ti (see Fig. 1), of which Ni and Co are two metals to consider in the occupational health risk assessment. According to the Classification, Labelling and Packaging (CLP) regulation, Ni powders (particle diameter $<1 \text{ mm}$) are classified for Skin Sens.1 (may cause an allergic skin reaction), Carc. 2 (suspected of causing cancer) and STOT RE 1 (causes damage to organs) [55]. No classification exists for Co metal powder, but Co metal is classified as Skin Sens.1 and Resp. Sens. 1B (may cause asthma or breathing difficulties if inhaled) [56]. Dissolved alloy constituents were not released as particles but rather as ions that readily, as e.g. shown for Co and Ni [57], are expected to form strong complexes in both ALF and in cell media. In this study, 0.17–0.19 $\mu\text{g Ni}/\mu\text{g}$ and 0.08–0.09 $\mu\text{g Co}/\mu\text{g}$ were released from 18Ni300 into ALF after 24 h of exposure. Compared to the release of Ni and Co from other Fe- and Ni-based alloy powders exposed in ALF up to 168 h reported in a previous study [57], the 18Ni300 powders showed substantially higher (up to 2000-fold for Ni, and 3000-fold for Co) released amounts after 24 h exposure. The fact that no toxicity was observed for the completely dissolved 18Ni300 powders despite the release of both Co and Ni in ALF, may be related to rapid changes in metal speciation of released Co and Ni forming metal complexes with ligands of the ALF medium that are not very well taken up by the cells. Complexation of released metals is also expected to take place in the cell medium. Predictions of the chemical speciation of released Co and Ni in cell medium (DMEM) and of Ni in ALF show no free ions or labile complexes but the predominance of strongly bonded metal complexes with cell medium constituents [53,54,58].

This study revealed material-specific changes between virgin and non-fused reused powders used in AM using powder bed fusion with selective laser melting. A higher fraction of single-crystalline particles of ferritic microstructure was observed within the reused powder particles of 316L compared to the virgin powder. Such particles are known to form upon very rapid cooling and thereby change the magnetic properties of the powder. This was also the case for the reused powder as well as changes in surface composition and, most importantly, both its extent of metal release and corrosion behavior. This was less evident for the other two alloy powders (IN718-passive alloy and 18Ni300-active alloy) even though slight differences in surface oxide composition and extent of metal release also were observed for IN718, and complete dissolution was observed for 18Ni300. An increased corrosion susceptibility has previously been reported for the magnetic fraction of $<45 \mu\text{m}$ gas-atomized 316L powders when compared to its non-magnetic counterpart [34]. A possible explanation is the enrichment of Mn and reduced content of Cr in the surface oxide after rapid solidification, which can result in a less passive surface oxide [34]. Another possible explanation is a larger fraction of amorphous versus crystalline oxides within the outermost surface [34,59], which can increase complexation-induced dissolution in ALF [60].

Further studies should investigate nano-sized airborne particles generated during AM procedures.

4. Conclusion

This study investigated differences between virgin and reused common metal alloy powders (316L, 18Ni300 and IN718) used in AM powder bed fusion (with selective laser melting) from a physico-chemical, microstructural, particle stability, surface oxide composition, bioaccessibility, and *in-vitro* toxicity (towards cultured human lung cells) perspective. The following main conclusions were drawn:

- 1 For the IN718 and 18Ni300 alloy powders, the non-fused reused (and dust) powders showed no, or only minor, differences compared with virgin powders in terms of particle size distribution, surface composition, magnetic properties, corrosion performance or bioaccessibility in ALF. In contrast, the laser melting process induced an increased fraction of single-crystalline ferritic 316L particles observed for the reused powder. This increased the ferromagnetic properties of the powder and resulted in more agglomeration, increased hydrodynamic size and extent of metal release in ALF as well as lower corrosion resistance compared with the virgin 316L powder.
- 2 The high strength alloy powder 18Ni300 dissolved almost completely after exposure to ALF for 24 h at 37 °C, for both the virgin, reused, and dust powders. This alloy powder further showed an active corrosion behavior in ALF. In contrast, the 316L and IN718 alloy powders showed a passive behavior (high corrosion resistance) and less than 1 wt. % (316L) and 0.1% (IN718) of their metal constituents dissolved into ALF within 24 h.
- 3 None of the powders showed any cytotoxicity towards human bronchial epithelial cells (10–100 $\mu\text{g}/\text{mL}$, 24–48 h) or any ability to generate reactive oxygen species *in-vitro* conditions. Since Ni and Co metal powders are classified as respirable and skin sensitizers, reproductive toxins, and possible carcinogens, further studies are required to determine long-term cytotoxic and genotoxic effects, and other potential health hazards. High released amounts of Ni and Co in ALF (0.17–0.19 $\mu\text{g Ni}/\mu\text{g}$ and 0.08–0.09 $\mu\text{g Co}/\mu\text{g}$) were observed for the 18Ni300 powder.

Declaration of Competing Interest

The authors declare that they have no known competing financial interests or personal relationships that could have appeared to influence the work reported in this paper.

Funding

This work was supported by the Swedish Governmental Agency for Innovation Systems Vinnova [Grant No. 2018-03336]; the Swedish Research Council [Grant Nos. 2015-04177, 2019-03657]; the Canada Research Chairs Program [Grant No. 950 – 233099]; the Canada Wolfe-Western Fellowship [Grant No. 2020]; and KTH faculty grants and the China Scholarship Council [Grant No. 201700260221].

Acknowledgments

We thank Oskar Karlsson, Swerim AB, for EBSD measurements. We thank the AM workshop at Siemens for contributing with knowledge and powder samples.

Supplementary materials

Supplementary material associated with this article can be found, in the online version, at [doi:10.1016/j.mtla.2021.101196](https://doi.org/10.1016/j.mtla.2021.101196).

References

- [1] P.K. Gokuldoss, S. Kolla, J. Eckert, Additive manufacturing processes: selective laser melting, electron beam melting and binder jetting—selection guidelines, *Materials* 10 (6) (2017) 672.

- [2] D. Herzog, V. Seyda, E. Wycisk, C. Emmelmann, Additive manufacturing of metals, *Acta Mater.* 117 (2016) 371–392.
- [3] C. Emmelmann, P. Scheinmann, M. Munsch, V. Seyda, Laser additive manufacturing of modified implant surfaces with osseointegrative characteristics, *Phys. Procedia* 12 (2011) 375–384.
- [4] J.P. Kruth, B. Vandenbroucke, J. Van Vaerenbergh, I. Naert, in: Rapid manufacturing of dental prostheses by means of selective laser sintering/melting, S4, Paris, France, 2005, pp. 176–186.
- [5] D. Appleyard, Powering up on powder technology, *Met. Powder Rep.* 70 (6) (2015) 285–289.
- [6] S.M. Thompson, L. Bian, N. Shamsaei, A. Yadollahi, An overview of direct laser deposition for additive manufacturing; part I: transport phenomena, modeling and diagnostics, *Addit. Manuf.* 8 (2015) 36–62.
- [7] M.J. Heiden, L.A. Deibler, J.M. Rodelas, J.R. Koepke, D.J. Tung, D.J. Saiz, B.H. Jared, Evolution of 316L stainless steel feedstock due to laser powder bed fusion process, *Addit. Manuf.* 25 (2019) 84–103.
- [8] J.A. Slotwinski, E.J. Garboczi, P.E. Stutzman, C.F. Ferraris, S.S. Watson, M.A. Peltz, Characterization of metal powders used for additive manufacturing, *J. Res. Natl. Inst. Stand. Technol.* 119 (2014) 460.
- [9] P. Mellin, R. Shvab, A. Strondl, M. Randelius, H. Brodin, E. Hryha, L. Nyborg, COP-GLOW and XPS investigation of recycled metal powder for selective laser melting, *Powder Metall.* 60 (3) (2017) 223–231.
- [10] P. Nandwana, W.H. Peter, R.R. Dehoff, L.E. Lowe, M.M. Kirka, F. Medina, S.S. Babu, Recyclability study on Inconel 718 and Ti-6Al-4V powders for use in electron beam melting, *Metall. Mater. Trans. B* 47 (1) (2016) 754–762.
- [11] A. Hadadzadeh, C. Baxter, B.S. Amirkhiz, M. Mohammadi, Strengthening mechanisms in direct metal laser sintered AlSi10Mg: Comparison between virgin and recycled powders, *Addit. Manuf.* 23 (2018) 108–120.
- [12] J. Yan, Y. Zhou, R. Gu, X. Zhang, W.M. Quach, M. Yan, A comprehensive study of steel powders (316L, H13, P20 and 18Ni300) for their selective laser melting additive manufacturing, *Metals* 9 (1) (2019) 86.
- [13] H. Tang, M. Qian, N. Liu, X. Zhang, G. Yang, J. Wang, Effect of powder reuse times on additive manufacturing of Ti-6Al-4V by selective electron beam melting, *JOM* 67 (3) (2015) 555–563.
- [14] F. Pinto, I. Souza Filho, M. Sandim, H. Sandim, Defects in parts manufactured by selective laser melting caused by δ -ferrite in reused 316L steel powder feedstock, *Addit. Manuf.* 31 (2020) 100979.
- [15] N. Gorji, R. O'Connor, D. Brabazon, XPS, XRD, and SEM characterization of the virgin and recycled metallic powders for 3D printing applications, *IOP. Conf. Ser. Mater. Sci. Eng.* 591 (2019) 012016.
- [16] N.E. Gorji, R. O'Connor, A. Mussatto, M. Snelgrove, P.M. González, D. Brabazon, Recyclability of stainless steel (316 L) powder within the additive manufacturing process, *Materialia* 8 (2019) 100489.
- [17] E. Buranská, I. Buranský, L. Morović, K. Liška, Environment and safety impacts of additive manufacturing: a review, *Vedecké Práce Materiálovotechnologickej Fakulty Slovenskej Technickej Univerzity v Bratislave so Sídrom v Trnave* 27 (44) (2019) 9–20.
- [18] F. Chan, R. House, I. Kudla, J. Lipszyc, N. Rajaram, S. Tarlo, Health survey of employees regularly using 3D printers, *Occup. Med.* 68 (3) (2018) 211–214.
- [19] G.A. Roth, C.L. Geraci, A. Stefaniak, V. Murashov, J. Howard, Potential occupational hazards of additive manufacturing, *J. Occup. Environ. Hyg.* 16 (5) (2019) 321–328.
- [20] R. House, N. Rajaram, S. Tarlo, Case report of asthma associated with 3D printing, *Occup. Med.* 67 (8) (2017) 652–654.
- [21] A.J. Väisänen, M. Hyttinen, S. Ylönen, L. Alonen, Occupational exposure to gaseous and particulate contaminants originating from additive manufacturing of liquid, powdered, and filament plastic materials and related post-processes, *J. Occup. Environ. Hyg.* 16 (3) (2019) 258–271.
- [22] European Chemicals Agency, Hazard classification & labelling. <https://echa.europa.eu/de/substance-information/-/substanceinfo/100.028.283>, 2021 (accessed on 2021-08-18).
- [23] European Chemicals Agency, Hazard classification & labelling. <https://echa.europa.eu/sv/substance-information/-/substanceinfo/100.028.325>, 2021 (accessed on 2021-08-18).
- [24] N. Guha, D. Loomis, K.Z. Guyton, Y. Grosse, F. El Ghissassi, V. Bouvard, L. Benbrahim-Tallaa, N. Vilahur, K. Muller, K. Straif, Carcinogenicity of welding, molybdenum trioxide, and indium tin oxide, *Lancet Oncol.* 18 (5) (2017) 581–582.
- [25] M.K. Honaryar, R.M. Lunn, D. Luce, W. Ahrens, J. Hansen, L. Bouaoun, D. Loomis, G. Byrnes, N. Vilahur, L. Stayner, Welding fumes and lung cancer: a meta-analysis of case-control and cohort studies, *Occup. Environ. Med.* 76 (6) (2019) 422–431.
- [26] Finnish Institute of Occupational Health, Control Approach - Chemical safety of 3D printing at workplaces. <http://mb.cision.com/Public/5751/2134887/86ab1364ec6d8361.pdf>, 2016 (accessed on 2021-08-18).
- [27] D. Rejeski, F. Zhao, Y. Huang, Research needs and recommendations on environmental implications of additive manufacturing, *Addit. Manuf.* 19 (2018) 21–28.
- [28] X. Wang, G. Herting, Z. Wei, I. Odnevall Wallinder, Y. Hedberg, Bioaccessibility of nickel and cobalt in powders and massive forms of stainless steel, nickel-or cobalt-based alloys, and nickel and cobalt metals in artificial sweat, *Regul. Toxicol. Pharmacol.* 106 (2019) 15–26.
- [29] N. Lombaert, C. Mackie, V. Verougstraete, T. Brouwers, F. Van Assche, A. Oller, Use of bioelution as a screening tool for characterisation of substances, *Am. J. Anal. Chem.* 9 (03) (2018) 134.
- [30] United Nations, The Globally harmonized system of classification and labeling of chemicals, Annex 10, guidance document on transformation/dissolution of metals and metal compounds in aqueous media. https://www.unsceo.org/fileadmin/DAM/trans/danger/publi/ghs/ghs_rev07/English/13e_annex10.pdf, 2017 (accessed on 2021-08-18).
- [31] K. Midander, J. Pan, C. Leygraf, Elaboration of a test method for the study of metal release from stainless steel particles in artificial biological media, *Corros. Sci.* 48 (9) (2006) 2855–2866.
- [32] Y. Hedberg, J. Gustafsson, H.L. Karlsson, L. Möller, I. Odnevall Wallinder, Bioaccessibility, bioavailability and toxicity of commercially relevant iron-and chromium-based particles: *in vitro* studies with an inhalation perspective, *Part Fibre Toxicol.* 7 (1) (2010) 23.
- [33] W. Stopford, J. Turner, D. Cappellini, T. Brock, Bioaccessibility testing of cobalt compounds, *J. Environ. Monit.* 5 (4) (2003) 675–680.
- [34] Y. Hedberg, M. Norell, P. Linhardt, H. Bergqvist, I. Odnevall Wallinder, Influence of surface oxide characteristics and speciation on corrosion, electrochemical properties and metal release of atomized 316L stainless steel powders, *Int. J. Electrochem. Sc.* 7 (12) (2012) 11655–11677.
- [35] S. McCarrick, Z. Wei, N. Moelijker, R. Derr, K.A. Persson, G. Hendriks, I. Odnevall Wallinder, Y. Hedberg, H.L. Karlsson, High variability in toxicity of welding fume nanoparticles from stainless steel in lung cells and reporter cell lines: the role of particle reactivity and solubility, *Nanotoxicology* 13 (10) (2019) 1293–1309.
- [36] G. Oberdörster, E. Oberdörster, J. Oberdörster, Nanotoxicology: an emerging discipline evolving from studies of ultrafine particles, *Environ. Health Perspect.* 113 (7) (2005) 823–839.
- [37] Y. Hedberg, O. Karlsson, P. Szakalos, I. Odnevall Wallinder, Ultrafine 316 L stainless steel particles with frozen-in magnetic structures characterized by means of electron backscattered diffraction, *Mater. Lett.* 65 (14) (2011) 2089–2092.
- [38] Z. Sun, X. Tan, S.B. Tor, W.Y. Yeong, Selective laser melting of stainless steel 316L with low porosity and high build rates, *Mater. Des.* 104 (2016) 197–204.
- [39] M.C. Biesinger, B.P. Payne, A.P. Grosvenor, L.W. Lau, A.R. Gerson, R.S.C. Smart, Resolving surface chemical states in XPS analysis of first row transition metals, oxides and hydroxides: Cr, Mn, Fe, Co and Ni, *Appl. Surf. Sci.* 257 (7) (2011) 2717–2730.
- [40] N.E. Gorji, P. Saxena, M.R. Corfield, A. Clare, J.P. Rueff, J. Bogan, P.G. González, M. Snelgrove, G. Hughes, R. O'Connor, A new method for assessing the recyclability of powders within powder bed fusion process, *Mater. Charact.* 161 (2020) 110167.
- [41] L. Ardila, F. Garciañda, J. González-Díaz, P. Álvarez, A. Echeverría, M. Petite, R. Defley, J. Ochoa, Effect of IN718 recycled powder reuse on properties of parts manufactured by means of selective laser melting, *Phys. Proc.* 56 (2014) 99–107.
- [42] M.C. Biesinger, L.W. Lau, A.R. Gerson, R.S.C. Smart, Resolving surface chemical states in XPS analysis of first row transition metals, oxides and hydroxides: Sc, Ti, V, Cu and Zn, *Appl. Surf. Sci.* 257 (3) (2010) 887–898.
- [43] Biesinger M.C., X-ray Photoelectron Spectroscopy (XPS) Reference Pages. <http://www.xpsfitting.com/>, 2009 (accessed on 2020-08-18).
- [44] M. Renderos, A. Torregaray, M.E. Gutierrez-Orrantia, A. Lamikiz, N. Saintier, F. Giro, Microstructure characterization of recycled IN718 powder and resulting laser clad material, *Mater. Charact.* 134 (2017) 103–113.
- [45] Y. Hedberg, J. Gustafsson, H.L. Karlsson, L. Möller, I. Odnevall Wallinder, Bioaccessibility, bioavailability and toxicity of commercially relevant iron-and chromium-based particles: *in vitro* studies with an inhalation perspective, *Part Fibre Toxicol.* 7 (1) (2010) 23.
- [46] Y.S. Hedberg, G. Herting, S. Latvala, K. Elihn, H.L. Karlsson, I. Odnevall Wallinder, Surface passivity largely governs the bioaccessibility of nickel-based powder particles at human exposure conditions, *Regul. Toxicol. Pharmacol.* 81 (2016) 162–170.
- [47] H. Stockmann-Juvala, Y. Hedberg, N. Dhinsa, D. Griffiths, P. Brooks, A. Zitting, I. Odnevall Wallinder, T. Santonen, Inhalation toxicity of 316L stainless steel powder in relation to bioaccessibility, *Hum. Exp. Toxicol.* 32 (11) (2013) 1137–1154.
- [48] S.A. Jlungren, H. Karlsson, B. Ståhlbom, B. Krapf, L. Fornander, L.E. Karlsson, B. Bergström, E. Nordenberg, T.K. Ervik, P. Graff, Biomonitoring of metal exposure during additive manufacturing (3D printing), *Saf. Health Work* 10 (4) (2019) 518–526.
- [49] A.R. Gliga, S. Skoglund, I. Odnevall Wallinder, B. Fadeel, H.L. Karlsson, Size-dependent cytotoxicity of silver nanoparticles in human lung cells: the role of cellular uptake, agglomeration and Ag release, *Part Fibre Toxicol.* 11 (1) (2014) 1–17.
- [50] K. Midander, P. Cronholm, H.L. Karlsson, K. Elihn, L. Möller, C. Leygraf, I. Odnevall Wallinder, Surface characteristics, copper release, and toxicity of nano- and micrometer-sized copper and copper (II) oxide particles: a cross-disciplinary study, *Small* 5 (3) (2009) 389–399.
- [51] G. Oberdörster, A. Maynard, K. Donaldson, V. Castranova, J. Fitzpatrick, K. Ausman, J. Carter, B. Karn, W. Kreyling, D. Lai, Principles for characterizing the potential human health effects from exposure to nanomaterials: elements of a screening strategy, *Part Fibre Toxicol.* 2 (1) (2005) 8.
- [52] Y.S. Hedberg, S. Pradhan, F. Cappellini, M.-E. Karlsson, E. Blomberg, H. Karlsson, I. Odnevall Wallinder, J.F. Hedberg, Electrochemical surface oxide characteristics of metal nanoparticles (Mn, Cu and Al) and the relation to toxicity, *Electrochim. Acta.* 212 (2016) 360–371.
- [53] S. Latvala, J. Hedberg, S. Di Bucchianico, L. Möller, I. Odnevall Wallinder, K. Elihn, H.L. Karlsson, Nickel release, ROS generation and toxicity of Ni and NiO micro- and nanoparticles, *PLoS One* 11 (7) (2016) e0159684.
- [54] F. Cappellini, Y. Hedberg, S. McCarrick, J. Hedberg, R. Derr, G. Hendriks, I. Odnevall Wallinder, H.L. Karlsson, Mechanistic insight into reactivity and (geno) toxicity of well-characterized nanoparticles of cobalt metal and oxides, *Nanotoxicology* 12 (6) (2018) 602–620.
- [55] European Chemicals Agency, Harmonised classification - annex VI of regulation (EC) No 1272/2008 (CLP regulation). <https://echa.europa.eu/de/information-on-chemicals/cl-inventory-database/-/discli/details/133816>, 2008 (accessed on 2021-08-18).
- [56] European Chemicals Agency, Harmonised classification - annex VI of regulation (EC) No 1272/2008 (CLP regulation). <https://echa.europa.eu/information>

- on-chemicals/cl-inventory-database/-/discli/details/34808, 2008 (accessed on 2021-08-18).
- [57] X. Wang, I. Odnevall Wallinder, Y. Hedberg, Bioaccessibility of nickel and cobalt released from occupationally relevant alloy and metal powders at simulated human exposure scenarios, *Ann. Work Expos. Health* 64 (6) (2020) 659–675.
- [58] Y. Hedberg, J. Hedberg, Y. Liu, I.O. Wallinder, Complexation-and ligand-induced metal release from 316L particles: importance of particle size and crystallographic structure, *BioMetals* 24 (6) (2011) 1099–1114.
- [59] Y. Hedberg, M. Norell, J. Hedberg, P. Szakálos, P. Linhardt, I. Odnevall Wallinder, Surface characterisation of fine inert gas and water atomised stainless steel 316L powders: formation of thermodynamically unstable surface oxide phases, *Powder Metall.* 56 (2) (2013) 158–163.
- [60] Y. Hedberg, K. Midander, Size matters: mechanism of metal release from 316L stainless steel particles is governed by size-dependent properties of the surface oxide, *Mater. Lett.* 122 (2014) 223–226.